Published in final edited form as:
J Biomech Eng. 2009 January ; 131(1): 011013. doi:10.1115/1.3005147.

A Simple Mass-Spring Model with Roller Feet can induce the Ground Reactions Observed in Human Walking

Ben R. Whittington[1] and **Darryl G. Thelen**[1,2,3]

[1] Department of Mechanical Engineering, University of Wisconsin-Madison, Madison, WI

[2] Department of Biomedical Engineering, University of Wisconsin-Madison, Madison, WI

[3] Department of Orthopedics and Rehabilitation, University of Wisconsin-Madison, Madison, WI

Abstract

Background—It has previously been shown that a bipedal model consisting of a point mass supported by spring limbs can be tuned to simulate periodic human walking.

Method of Approach—In this study, we incorporated roller feet into the spring-mass model and evaluated the effect of roller radius, impact angle, and limb stiffness on spatio-temporal gait characteristics, ground reactions, and center of pressure excursions. We also evaluated the potential of the improved model to predict speed-dependent changes in ground reaction forces and center-of-pressure excursions observed during normal human walking.

Results—We were able to find limit cycles that exhibited gait-like motion across a wide spectrum of model parameters. Incorporation of the roller foot (R = 0.3 m) reduced the magnitude of peak ground reactions forces and allowed for forward center of pressure progression, making the model more consistent with human walking. At a fixed walking speed, increasing the limb impact angle reduced the cadence and prolonged stance duration. Increases in either limb stiffness or impact angle tended to result in more oscillatory vertical ground reactions. Simultaneous modulation of the limb impact angle and limb stiffness was needed to induce speed-related changes in ground reactions that were consistent with those measured during normal human walking, with better quantitative agreement achieved at slower speeds.

Conclusions—We conclude that a simple mass-spring model with roller feet can well describe ground reaction forces, and hence center of mass motion, observed during normal human walking.

Keywords

gait; dynamic simulation; limit cycle; limb stiffness

INTRODUCTION

Simple models of human walking have provided tremendous insights into the mechanics of gait, benefiting from the idea that “simplicity promotes understanding” [1]. The classic model of gait is an inverted pendulum, which is useful in describing the exchange between gravitational potential and kinetic energy during single support [2]. Compass models, consisting of two coupled inverted pendulums, can achieve stable limit cycles when walking down a slight (~3%) slope, demonstrating that passive dynamical properties lead naturally to bipedal walking patterns [1,3]. Simple ankle push-off actuation can be used to efficiently

Please address correspondence to: Darryl G. Thelen, Department of Mechanical Engineering, 1513 University Ave., Madison, WI 53706, Phone: (608) 262-1902, Fax: (608) 265-2316, thelen@engr.wisc.edu.

power a compass model on level ground [4], with the energetic requirements at varying speeds mimicking that seen in humans [5]. Further, the incorporation of roller feet on the inverted pendulum-type limbs [6] can account for the progression of the center of pressure (COP) under the human foot during stance [7]. While providing many important insights, it has long been recognized that inverted pendulum models are not good predictors of the ground reaction forces, and hence center-of-mass motion, throughout a normal gait cycle [8,9].

A recent study showed that a bipedal mass-spring model, which has classically been used to describe running [10], can also be tuned to reproduce the characteristic vertical and anterior-posterior (A-P) ground reaction forces observed during human walking [11]. However, the classic spring-mass model [10,12] has a point foot and therefore a fixed COP during stance. In contrast, a roller foot would allow for the COP to progress, thereby reducing the horizontal distance between the COP and center of mass (COM). Such an effect could potentially induce a more vertically oriented ground reaction force and hence smaller breaking and push-off forces during early and late phases of stance.

In this study, we developed and used a mass-spring model with roller feet to simulate human walking. The following three purposes were addressed with the model. First, we determined the effect of the roller foot on the ground reactions and COP excursions seen during stance. We hypothesized that increasing the roller foot radius would reduce A-P force magnitudes, while inducing center of pressure excursions that are more consistent with human gait. Our second purpose was to evaluate the effect of roller radius, limb impact angle and limb stiffness on cadence, step length, walking speed and induced ground reactions. The third purpose was to determine if modulation of limb stiffness and impact angle is sufficient to induce the speed-dependent changes in cadence, step length, ground reactions and center-of-pressure excursions seen in normal human walking.

METHODS

The model consisted of a point mass (M), two massless limb springs of stiffness K, and massless circular roller feet of radius R (Fig. 1). The base of each limb spring was rigidly fixed to its roller foot, such that a single angle (θ) defined the orientation of a limb and foot with respect to a vertical upright. The proximal end of the limb spring was pinned to the point mass. Thus, the configuration of each limb was described by a limb angle θ and spring length L.

Equations of motion (Eq. 1) for the model were derived in terms of the trailing limb (denoted by subscript 1) using a Lagrangian approach (Appendix A)

$$\begin{bmatrix} MR\sin\theta_1 & M \\ ML_1^2+2ML_1R\cos\theta_1+MR^2 & MR\sin\theta_1 \end{bmatrix} \begin{pmatrix} \ddot{\theta}_1 \\ \ddot{L}_1 \end{pmatrix} = \begin{bmatrix} -MR\dot{\theta}_1^2\cos\theta_1+ML_1\dot{\theta}_1^2+M\dot{\theta}_1^2R\cos\theta_1 - Mg\cos\theta_1 \\ +KL_0 - KL_1+(KL_0 - KL_2)\left(\frac{L_2\cos(\theta_1-\theta_2)+R\cos\theta_1}{L_2+R\cos\theta_2}\right) \\ -2ML_1\dot{L}_1\dot{\theta}_1 - 3M\dot{L}_1\dot{\theta}_1R\cos\theta_1+ML_1\dot{\theta}_1^2R\sin\theta_1+M\dot{L}_1R\dot{\theta}_1\cos\theta_1+MgL_1\sin\theta_1 \\ +(KL_0 - KL_2)\left(\frac{RL_2\sin\theta_2-L_1L_2\sin(\theta_1-\theta_2)-RL_1\sin\theta_1}{L_2+R\cos\theta_2}\right) \end{bmatrix} \quad (1)$$

where g represents the gravitational acceleration and L_0 represents the spring slack length.

For each simulation, the model was initially positioned in upright single support with the point mass at its apex and the swing limb positioned out in front of the stance limb at a prescribed impact angle (Fig. 2). During the initial single support period, the equations of motion (Eq. 1) were numerically integrated forward in time until contact of the leading limb with the ground was detected. We assumed that there was no slip between either of the rollers and ground during contact. As a result during double support, the closed loop kinematic constraints could be used to determine the forward limb spring velocity and rotational angular velocity (denoted by limb 2) as a function of the trailing limb states.

$$\begin{Bmatrix} \dot{L}_2 \\ \dot{\theta}_2 \end{Bmatrix} = \begin{bmatrix} \frac{L_2\cos(\theta_1-\theta_2)+R\cos\theta_1}{L_2+R\cos\theta_2} & \frac{RL_2\sin\theta_2-L_1L_2\sin(\theta_1-\theta_2)-RL_1\sin\theta_1}{L_2+R\cos\theta_2} \\ \frac{\sin(\theta_1-\theta_2)}{L_2+R\cos\theta_2} & \frac{R\cos\theta_2+L_1\cos(\theta_1-\theta_2)}{L_2+R\cos\theta_2} \end{bmatrix} \begin{Bmatrix} \dot{L}_1 \\ \dot{\theta}_1 \end{Bmatrix} \quad (2)$$

Differentiation of Eq. 2 resulted in the following relationship (Eq. 3) between the accelerations of the leading and trailing limbs during double support.

$$\begin{Bmatrix} \ddot{L}_2 \\ \ddot{\theta}_2 \end{Bmatrix} = \begin{bmatrix} \frac{L_2\dot{\theta}_1(L_2\dot{\theta}_2\cos(\theta_1-\theta_2)-\dot{L}_2\sin(\theta_1-\theta_2))}{\dot{\theta}_2^2} & \frac{-L_2(L_2\dot{\theta}_2L_1\dot{\theta}_1\sin(\theta_1-\theta_2)-L_2\dot{\theta}_2\dot{L}_1\cos(\theta_1-\theta_2)+\dot{L}_2L_1\dot{\theta}_1\cos(\theta_1-\theta_2)+\dot{L}_2\dot{L}_1\sin(\theta_1-\theta_2))}{\dot{\theta}_2^2} \\ \frac{\dot{\theta}_1\dot{\theta}_2\sin(\theta_1-\theta_2)}{L_2} & \frac{\dot{\theta}_2(L_1\dot{\theta}_1\cos(\theta_1-\theta_2)+\dot{L}_1\sin(\theta_1-\theta_2))}{L_2} \end{bmatrix} \begin{Bmatrix} \ddot{L}_1 \\ \ddot{\theta}_1 \end{Bmatrix} \quad (3)$$

Double support continued until the trailing limb spring reached its slack length. At this point, the trailing limb was then reset in front of the body at the limb impact angle (Fig. 2). This swing limb motion incurred no energetic cost since the limb and foot were assumed massless. Numerical integration continued into the subsequent single limb support phase until the leading limb reached an upright configuration, and the half cycle of gait was complete. Throughout this process, integration was stopped in the case of circumstances not representative of gait (i.e. takeoff in single limb support, falling backward, or the mass bottoming out). The total system energy (TE) for the conservative system was calculated by summing kinetic, spring potential, and gravitational potential energies (Eq. 4)

$$TE = \underbrace{\frac{1}{2}M|\vec{v}|^2}_{\text{(Kinetic)}} + \underbrace{\frac{1}{2}K(L_0-L_1)^2 + \frac{1}{2}K(L_0-L_2)^2}_{\text{(Spring Potential)}} + \underbrace{Mg(R+L_i\cos\theta_i)}_{\text{(Gravitational Potential)}} \quad (4)$$

where $\vec{v}$ is the velocity of the point mass (Eq. A.2, Appendix) and L_i and θ_i refer to a limb currently in contact.

Given a set of model parameters and desired walking speed, a nonlinear equation solver (fsolve, Matlab ®) was used to determine a set of initial states such that limit cycle behavior was achieved. Specifically, we solved for initial states of the trailing limb (L_1 (0), $\dot{\theta}_1(0)$) such that the states of the second limb at the end of the half-gait cycle matched the initial states of the first stance limb ($\dot{\theta}_2$ (t_f) = $\dot{\theta}_1$ (0), $L_2(t_f) = L_1(0)$) while also achieving the desired average walking speed. The limb spring velocity in the initial upright configuration was assumed to be zero for all simulations (i.e. $\dot{L}_1(0) = 0$). We evaluated the effect of limb stiffness (K), roller radius (R = 0.0, 0.1, 0.2, 0.3, and 0.4 m), and limb impact angle Θ on limit cycle behavior at slow (1.06 m/s), preferred (1.35 m/s), and fast (1.59m/s) walking speeds. The excursion of the center of pressure during stance was quantified by tracking the contact point of the roller foot with the ground. Ground reaction forces in the anterior-posterior (A-P) and vertical directions could then be computed at each time step using the

roller contact point, the spring deflection and the point mass location (Appendix B). Graphical representations of the solutions were used to evaluate the effects of model parameters on step length, cadence, total energy, COP excursions and ground reactions at parameter combinations where limit cycle solutions were found.

Comparison with Experimental Gait Data

Gait analysis was conducted on 20 healthy young subjects including 9 males (age 24±4, height 182±10 cm, weight 79±8 kg) and 11 females (age 24±3, height 166±10 cm, weight 58±13 kg). Subjects had no history of major orthopedic diagnosis, musculoskeletal trauma, or persistent joint pain. Each subject gave informed consent according to a protocol approved by the University of Wisconsin's Health Sciences Institutional Review Board. Subjects walked at three speeds (80%, 100%, and 120% of preferred) while their motion was tracked using a passive motion capture system and ground reaction forces were recorded at 2000 Hz from three imbedded force plates. Ground reaction data was used to identify heel contact and toe-off times. Ground reaction forces were then normalized to body mass and ensemble-averaged across subjects to obtain a representative set of ground reaction force curves for each of the walking speeds. Similarly, measured COP excursions were averaged to generate representative excursions for all three walking speeds. Spatio-temporal gait variables (stride length, gait speed, and cadence) were subsequently calculated from the measured kinematic data and compared to simulation results.

We generated simulations of a half gait cycle that were able to best replicate the ground reactions measured experimentally. This was done by first establishing regions within the solution space that led to simulations that were within one standard deviation of the cadence and step length measured experimentally at each speed. We then determined which parameter combinations within these regions induced ground reaction forces that best matched the average experimental forces. We used the sum of squared differences between the simulated and experimental ground reaction forces, normalized to the standard deviation of the experimental data, as the measure of goodness of fit.

RESULTS

At each walking speed, a large array of limit cycle solutions were found in which the system state at the end of a half gait cycle replicated the initial conditions at the start of the half gait cycle. Thus, each solution represented a periodic gait cycle during which constant total energy was maintained while energy transfer occurred between gravitational potential energy, elastic potential energy, and kinetic energy (Fig. 3).

Roller Radius Effect

As hypothesized, increasing the roller radius (while leaving other parameters constant) resulted in a decrease in both the peak vertical and AP ground reactions at a fixed walking speed (Fig. 4). Increasing roller radius also resulted in greater COP excursion with the change in excursion increasing approximately linearly with the radius of the roller.

Stiffness and Impact Angle Effects

With a fixed roller radius, the model was capable of walking at a fixed speed with different combinations of limb stiffness and impact angle (Fig. 5). Each solution corresponded to a specific step length (Fig. 5a), cadence (Fig. 5b) and total energy state (Fig. 5c). Increasing the limb impact angle resulted in longer step lengths, a reduction in cadence, and a decrease in total energy. Varying the limb stiffness had a smaller effect on the step length and cadence, but had a large effect on total energy, with a stiffer limb resulting in an increase in energy.

Variations in the impact angle and limb stiffness both had a substantial effect on the duration and magnitude of the ground reactions. An increase in impact angle at a constant stiffness resulted in a substantial increase in peak anterior-posterior and vertical ground reaction forces, and a longer stance period (Fig. 6). An increase in limb stiffness at a constant impact angle also acted to increase the peak A-P and vertical ground reactions, with the effect being more slightly pronounced at larger impact angles.

Using a fixed roller radius of 0.3 m, limit cycle solutions were found that were able to closely emulate the COP progression exhibited by the subjects at the slow, preferred and fast speeds (Fig. 7). Simultaneous increases in both the limb impact angle and limb stiffness resulted in the best agreement of the model predictions with the speed-related changes in ground reactions (Table 1). The smallest quantitative differences with average ground reactions were achieved at a slow walking speed (Fig. 7), with root mean squared (rms) differences of 2.8% and 6.7% body weight in the horizontal and vertical directions, respectively. At faster speeds, the simulated vertical force tended to exhibit greater oscillation during stance than that observed experimentally (Fig. 7). In addition, simulations at all three speeds predict a greater horizontal shear force on the leading limb during early stance than is observed experimentally.

DISCUSSION

This study demonstrates that a simple bipedal spring-mass model with roller feet can induce ground reactions, and hence center of mass motion, that emulate normal human walking. The classic inverted pendulum model can be seen as an extreme of the proposed mass-spring model in which the limb stiffness is made very high. An infinitely stiff limb would not absorb energy, leading to the loss of energy seen at heel contact in bipedal inverted pendulum models [3,5]. As a result, an energetic input is required in inverted pendulum models from either a down slope [1] or an impulsive push-off force [4] to maintain a repeatable walking cycle. While this step-to-step energetic demand has been correlated with the metabolic costs associated with walking [5], it is interesting to note that the proposed mass-spring model is able to walk on level ground with no external energy input. This is not to say that the model suggests that humans could walk with zero energy costs, since active modulation of muscle stiffness would be needed to maintain the constant limb stiffness. However, this energy expenditure would be distributed throughout the gait cycle, not just occurring at the step-to-step transitions. An additional noteworthy aspect of the proposed mass-spring model is its ability to represent a finite double support period. This is an improvement over compass models, in which step-to-step transitions occur instantaneously.

An improvement of the current mass-spring model over that proposed by Geyer [11] is the incorporation of a roller foot. We have shown that the roller produce two desirable effects that bring the simulated walking motion closer to that of humans. First the center of pressure (COP) naturally progresses from the heel to toe over stance phase. We found that a roller radius of 0.3m resulted in COP excursion that best agreed with experimental data at slow, preferred, and fast walking speeds (Fig. 7). This roller radius is similar to the 30% limb length measured by Hansen, *et. al.* [7]. The second important effect of the roller was a reduction in the magnitude of the A-P and vertical ground reaction forces during stance (Fig. 4), which better reflects the magnitude of forces seen in human walking (Fig. 7). The net ground reaction force in our model always points from the current COP to the center of mass of the model. Therefore, a reduction in the peak A-P forces is a natural consequence of allowing the COP to progress.

The model provides insights into possible mechanisms by which walking speed can be modulated. The strategy utilized by the model to facilitate speed variations similar to

humans involved the simultaneous modulation of the limb impact angle and limb stiffness. Based on sensitivity analyses, the larger impact angle is a primary mechanism to achieve longer steps and higher cadence at faster speeds (Fig. 5). Our simulations were able to closely replicate the COP progression at all speeds, and the vertical and A-P ground reactions at the slow and preferred speeds. However, the fast speed solution over-estimated the magnitude of both the negative A-P ground reaction force during early support and vertical force oscillation during stance (Fig. 7). This result could reflect two limitations associated with the model. First, while the model is restricted to sagittal plane motion, it is known that out of plane motion in human walking (ie. pelvic rotation) contributes to sagittal center of mass motion and step length [13]. The planar restriction may result in our model utilizing greater impact angles to achieve the experimentally observed step lengths. As mentioned previously, increasing impact angle leads to greater oscillation of the vertical ground reaction force (Fig. 6). Secondly, during human walking the swing limb is retracting during late swing which would diminish the negative A-P force at heel-strike. On the other hand, the swing limb of the model is stationary at heel-strike and thus over-estimates the deceleration that occurs during the first ~10% of stance (Fig. 7).

One needs to exercise caution when interpreting model variables in terms of specific joint variables measured during human walking. For example, the limb (spring) angle in the model does not strictly correspond to the hip joint angle. Instead, the limb angle represents the orientation of a line between the roller center and whole body center of mass. In human walking, this measure would be a function of pelvic, hip, knee and ankle joint angles. Similarly, the point mass in the model does not represent the hip center or any other fixed point on the body but rather the whole body center of mass. Further, the model has massless limbs and therefore does not simulate swing phase dynamics. Given the ballistic nature of swing phase, it is conceivable that this aspect could be added to the model, albeit at the expense of model simplicity.

The proposed mass-spring model of walking has a number of potential uses. First, the simplified model may provide a basis for controlling high degree of freedom walking models [14] and/or bipedal robots [15]. In particular, musculotendon stiffness could be actively modulated to achieve the desired stiffness of the limb, and hence the periodic movement pattern that it induces. Doing this would require that the posture dependent action of muscles be accounted for when reflecting muscle stiffness to limb stiffness. The Jacobian, relating muscle actions to end-point stiffness, could be used to efficiently compute this transformation [16]. Secondly, spring-mass models [11] have shown the ability to replicate other modes of locomotion such as running. An understanding of the parameters that generate different locomotion patterns could provide a unified framework for understanding gait transitions. A final use of the model would be to characterize an individual’s gait pattern using a minimal set of parameters (limb stiffness, impact angle, roller radius, energy level). The wide range of limit cycle walking solutions achievable by the simple mass-spring model could be exploited in distinguishing variations in human walking patterns. Such parameters could conceivably also be tracked over time, thereby providing a potential mechanism for tracking changes in gait associated with pathology, aging, or clinical interventions.

Acknowledgments

The authors would like to acknowledge Amy Silder and Bryan Heiderscheit for their contributions to walking data collection and processing. This work was supported by NIH AG24276.

NOMENCLATURE

M	point mass

g	gravitational acceleration
R	roller radius
K	limb stiffness
Θ	limb impact angle
H	center of mass height in upright unstretched configuration
TE	total system energy
L_0	spring resting length
L_i	limb length (trailing limb i = 1, leading limb i =2)
θ_i	limb angle
$\dot{L_i}$	limb linear velocity
$\dot{\theta_i}$	limb angular velocity
$\ddot{L}_i$	limb linear acceleration
$\ddot{\theta_i}$	limb angular acceleration
$\vec{v}$	point mass velocity
V	potential energy
T	kinetic energy
$\mathcal{L}$	Lagrangian

BIBLIOGRAPHY

1. McGeer T. Passive Dynamic Walking. The International Journal of Robotics Research 1990;9(2): 62–82.
2. Cavagna GA, Thys H, Zamboni A. The Sources of External Work in Level Walking and Running. The Journal of physiology 1976;262(3):639–657. [PubMed: 1011078]
3. Garcia M, Chatterjee A, Ruina A, Coleman M. The Simplest Walking Model: Stability, Complexity, and Scaling. J Biomech Eng 1998;120(2):281–288. [PubMed: 10412391]
4. Kuo AD. Energetics of Actively Powered Locomotion Using the Simplest Walking Model. J Biomech Eng 2002;124(1):113–120. [PubMed: 11871597]
5. Kuo AD, Donelan JM, Ruina A. Energetic Consequences of Walking Like an Inverted Pendulum: Step-to-Step Transitions. Exerc Sport Sci Rev 2005;33(2):88–97. [PubMed: 15821430]
6. Adamczyk PG, Collins SH, Kuo AD. The Advantages of a Rolling Foot in Human Walking. J Exp Biol 2006;209(Pt 20):3953–3963. [PubMed: 17023589]
7. Hansen AH, Childress DS, Knox EH. Roll-over Shapes of Human Locomotor Systems: Effects of Walking Speed. Clin Biomech (Bristol, Avon) 2004;19(4):407–414.
8. Buczek FL, Cooney KM, Walker MR, Rainbow MJ, Concha MC, Sanders JO. Performance of an Inverted Pendulum Model Directly Applied to Normal Human Gait. Clin Biomech (Bristol, Avon) 2006;21(3):288–296.
9. Mochon S, McMahon TA. Ballistic Walking. J Biomech 1980;13:49–57. [PubMed: 7354094]
10. McMahon TA, Cheng GC. The Mechanics of Running: How Does Stiffness Couple with Speed? J Biomech 1990;23(Suppl 1):65–78. [PubMed: 2081746]
11. Geyer H, Seyfarth A, Blickhan R. Compliant Leg Behaviour Explains Basic Dynamics of Walking and Running. Proceedings 2006;273(1603):2861–2867. [PubMed: 17015312]
12. Geyer H, Seyfarth A, Blickhan R. Spring-Mass Running: Simple Approximate Solution and Application to Gait Stability. Journal of theoretical biology 2005;232(3):315–328. [PubMed: 15572057]

13. Kerrigan DC, Riley PO, Lelas JL, Della Croce U. Quantification of Pelvic Rotation as a Determinant of Gait. Arch Phys Med Rehabil 2001;82(2):217–220. [PubMed: 11239313]

14. Delp SL, Loan JP, Hoy MG, Zajac FE, Topp EL, Rosen JM. An Interactive Graphics-Based Model of the Lower Extremity to Study Orthopaedic Surgical Procedures. IEEE Trans Biomed Eng 1990;37(8):757–767. [PubMed: 2210784]

15. Collins S, Ruina A, Tedrake R, Wisse M. Efficient Bipedal Robots Based on Passive-Dynamic Walkers. Science (New York, NY 2005;307(5712):1082–1085.

16. Hogan, N. Mechanical Impedance of Single- and Multi-Articular Systems. In: Winters, JM.; Woo, SL-Y., editors. Multiple Muscle Systems: Biomechanics and Movement Organization. Springer-Verlag; New York: 1990. p. 149-164.

APPENDIX

Appendix A: Lagrangian Formulation of Equations of Motion

The equations of motion of the conservative mass-spring model (Fig. A1) were derived using a Lagrangian formulation.

The total potential energy, *V*, in the system includes the elastic energy stored in the springs and the gravitational energy associated with the height of the mass M:

$$V=\frac{1}{2}K(L_0-L_1)^2+\frac{1}{2}K(L_0-L_2)^2+(R+L_i\cos\theta_i)Mg \tag{A.1}$$

where *K* represents the spring stiffness, L_0 represents the unstretched spring lengths, L_1 represents the trailing spring length, L_2 represents the leading spring length, R represents the roller radius, M represents the point mass, g is the gravitational constant, and L_i and θ_i refer to a limb currently in contact.

The velocity, $\vec{v}$, of the point mass M can be conveniently expressed via components directed both perpendicular ($\vec{e}_{\theta_1}$) and parallel ($\vec{e}_{L_1}$) to the trailing limb:

$$\vec{v}=\left(L_1\dot{\theta}_1+R\dot{\theta}_1\cos\theta_1\right)\vec{e}_{\theta_1}+\left(\dot{L}_1+R\dot{\theta}_1\sin\theta_1\right)\vec{e}_{L_1} \tag{A.2}$$

where θ_1 represents the angular velocity of the trailing limb. The total kinetic energy, T, in the system is thus given by

$$T=\frac{1}{2}M\left[\left(L_1\dot{\theta}_1+R\dot{\theta}_1\cos\theta_1\right)^2+\left(\dot{L}_1+R\dot{\theta}_1\sin\theta_1\right)^2\right] \tag{A.3}$$

The potential and kineatic energy expressions can be combined to form the Lagrangian, $\mathcal{L}=T-V$, of the system which is a function of the limb lengths (L_1, L_2) and the trailing limb angle θ_1.

$$\mathcal{L}=\frac{1}{2}M\left(L_1^2\dot{\theta}_1^2+2L_1\dot{\theta}_1^2R\cos\theta_1+\dot{L}_1^2+2\dot{L}_1R\dot{\theta}_1\sin\theta_1+R^2\dot{\theta}_1^2\right)-MgR+MgL_1\cos\theta_1+KL_0^2-KL_0L_1+\frac{1}{2}KL_1^2-KL_0L_2+\frac{1}{2}KL_2^2 \tag{A.4}$$

However, the system possesses only two independent degrees of freedom such that the angular velocity and spring velocity of the leading limb can be described in terms of the respective velocities of the trailing limb (Eq. 2 from text). The Jacobian terms describing incremental changes in L_2 as a function of L_1 and θ_1 can be taken directly from this relationship and are given by:

$$\frac{\partial L_2}{\partial L_1}=\frac{L_2\cos(\theta_1-\theta_2)+R\cos\theta_1}{L_2+R\cos\theta_2} \tag{A.5}$$

$$\frac{\partial L_2}{\partial \theta_1}=\frac{RL_2\sin\theta_2-L_1L_2\sin(\theta_1-\theta_2)-RL_1\sin\theta_1}{L_2+R\cos\theta_2} \tag{A.6}$$

This general Lagrangian equations of motion are given by:

$$\frac{d}{dt}\left(\frac{\partial \mathcal{L}}{\partial \dot{L}_1}\right)-\left[\frac{\partial \mathcal{L}}{\partial L_1}+\frac{\partial \mathcal{L}}{\partial L_2}\left(\frac{\partial L_2}{\partial L_1}\right)\right]=0 \tag{A.7}$$

$$\frac{d}{dt}\left(\frac{\partial \mathcal{L}}{\partial \dot{\theta}_1}\right)-\left[\frac{\partial \mathcal{L}}{\partial \theta_1}+\frac{\partial \mathcal{L}}{\partial L_2}\left(\frac{\partial L_2}{\partial \theta_1}\right)\right]=0 \tag{A.8}$$

Substituting equations (A.4, A.5 and A.6) into equations A.7 and A.8 results in the system equations of motion:

$$M\left(\ddot{L}_1+R\ddot{\theta}_1\sin\theta_1+R\dot{\theta}_1^2\cos\theta_1\right)-ML_1\dot{\theta}_1^2-M\dot{\theta}_1^2R\cos\theta_1+Mg\cos\theta_1-KL_0+KL_1-(KL_0-KL_2)\left(\frac{L_2\cos(\theta_1-\theta_2)+R\cos\theta_1}{L_2+R\cos\theta_2}\right)=0 \tag{A.9}$$

$$\begin{aligned}
&ML_1^2\ddot{\theta}_1+2ML_1\ddot{\theta}_1R\cos\theta_1\\
&\quad+MR^2\ddot{\theta}_1\\
&\quad+M\ddot{L}_1R\sin\theta_1\\
&\quad+2ML_1\dot{L}_1\dot{\theta}_1\\
&\quad+3M\,\dot{L}_1\dot{\theta}_1R\cos\theta_1\\
&\quad-ML_1\dot{\theta}_1^2R\sin\theta_1\\
&\quad-M\,\dot{L}_1R\dot{\theta}_1\cos\theta_1\\
&\quad-MgL_1\sin\theta_1\\
&\quad-(KL_0-KL_2)\left(\frac{RL_2\sin\theta_2-L_1L_2\sin(\theta_1-\theta_2)-RL_1\sin\theta_1}{L_2+R\cos\theta_2}\right)=0
\end{aligned} \tag{A.10}$$

The equations can then be rewritten in matrix form as a pair of coupled nonlinear second order differential equations (see Eq. 1). These two equations of motion are sufficient to

describe the dynamics during both single and double support. During single support, the massless non-contact limb is set to the limb impact angle and maintained there. During double support, the closed loop kinematic coupling allows for the motion of the leading limb to be computed given the positions, velocities and acceleration of the trailing limb (see eq. 2 and 3).

Appendix B: Calculation of Ground Reaction Force

The vertical and anterior-posterior (A-P) ground reaction forces attributable to each limb can be calculated by recognizing that the line of action of each limb force points from the COP to the center of mass (Fig. B1). Thus, the angle of the ground force vector, φ, for each limb is given by:

$$\varphi=\tan^{-1}\left(\frac{L\sin\theta}{R+L\cos\theta}\right) \tag{B.1}$$

The component of the ground reaction force vector acting along the limb spring, F_L, is simply the spring force:

$$F_L=K(L_0-L) \tag{B.2}$$

Knowing F_L and the ground force vector direction, the force perpendicular to the limb spring, F_θ, can then be determined:

$$F_\theta=-F_L\tan(\theta-\varphi) \tag{B.3}$$

The forces F_L and F_θ are then transformed into the ground reference frame to determine the forces acting in the fore-aft (F_x) and vertical (F_y) directions:

$$F_x=\sqrt{F_L^2+F_\theta^2}\sin(\varphi) \tag{B.4}$$

$$F_y=\sqrt{F_L^2+F_\theta^2}\cos(\varphi) \tag{B.5}$$

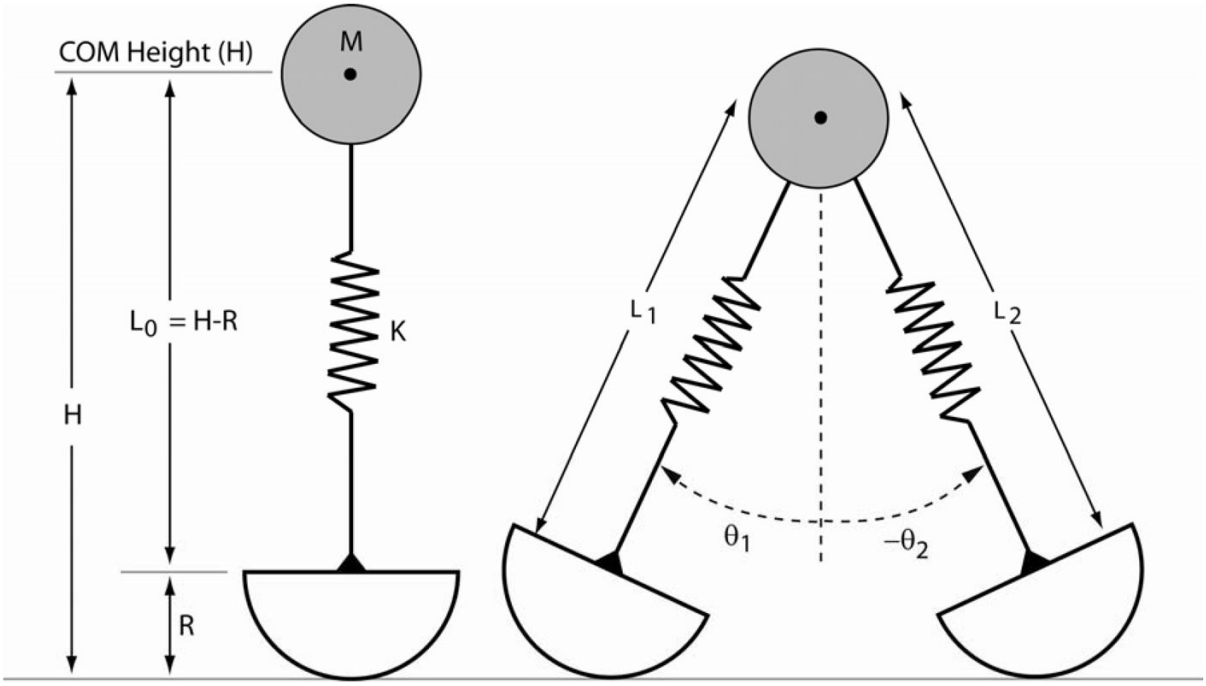

Figure 1.
Each limb was represented by a translational spring, with stiffness *K* and slack length L_o, that was rigidly coupled to a roller of radius *R* on one side and pinned to a point mass *M* on the other side. The point mass was assumed to be at the height *H* of the center of mass of the body with the limb spring in an unstretched upright configuration. Simulations were performed assuming normative values *H=1m* and *M=80 kg*. Roller radii of 0.0, 0.1, 0.2, 0.3, and 0.4 m were considered.

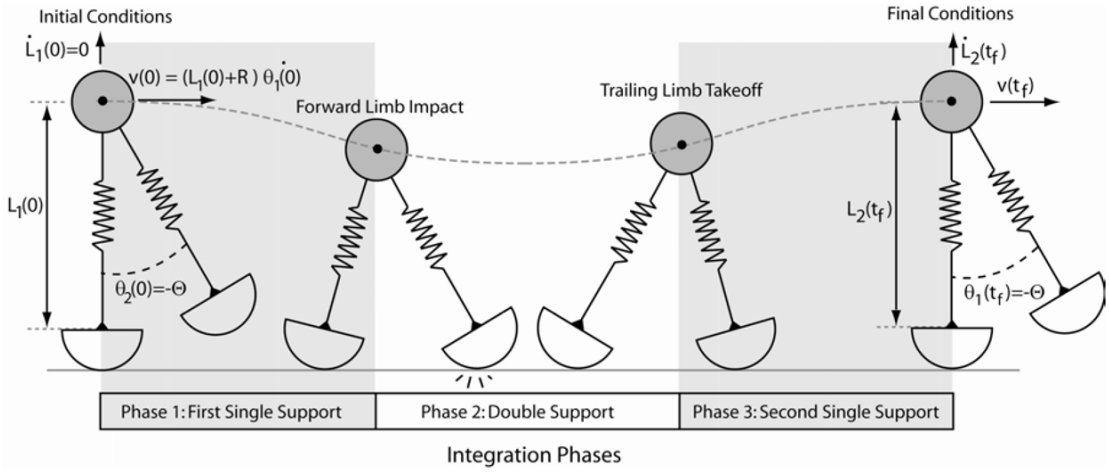

Figure 2.

Simulations were started with the trailing limb in an upright configuration and the forward limb oriented at the impact angle. The double support phase started when the leading limb contacted the ground, and then continued until the trailing limb length reached its undeflected length. The second single support phase continued until the limb reached an upright configuration, signaling the end of the half-gait cycle. We searched for limit cycle solutions in which the limb length, forward velocity and vertical velocity at the end of the half-gait cycle replicated the initial conditions.

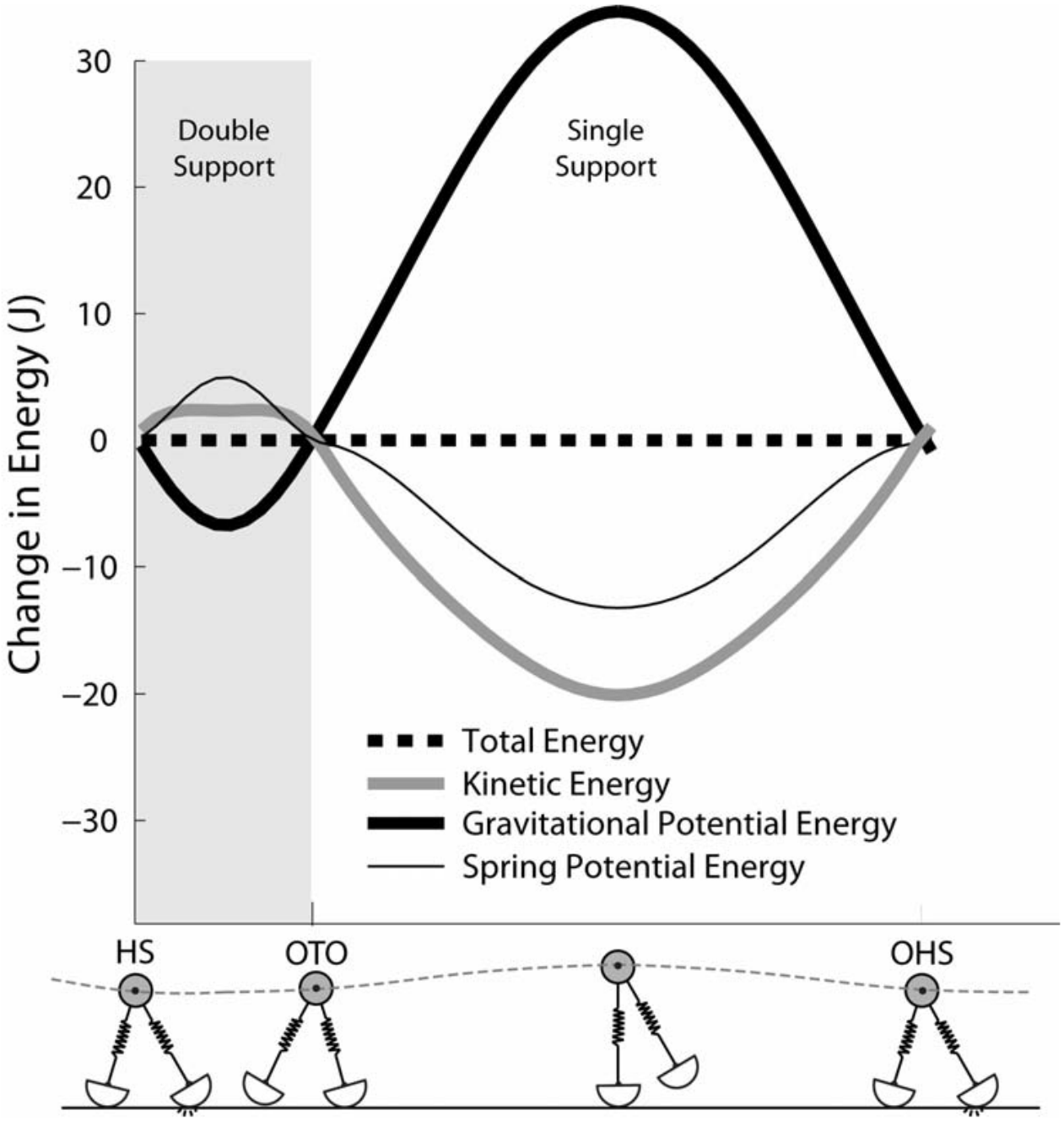

Figure 3.

The simple mass-spring model of walking is conservative, such that there was no change in total energy across a half gait cycle. The increase in gravitational potential energy during the first half of single support occurs as a result of both limb spring lengthening (decrease in spring potential energy) and a reduction in forward velocity (decrease in kinetic energy). A 0.3 m radius roller was used to generate this 1.35 m/s walking speed simulation. Abbreviations: HS – heel strike, OTO – opposite toe-off, OHS – opposite heel strike

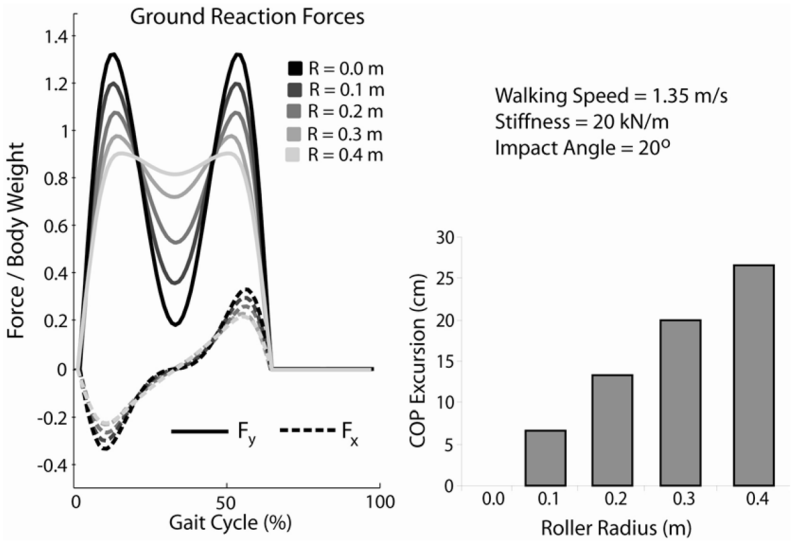

Figure 4.

Inclusion of a roller in the mass-spring model decreased the magnitude of the peak ground reaction forces in both the anterior (F_x) and vertical (F_y) directions. The forward progression of the center of pressure, as measured by the COP excursion during stance, increased approximately linearly with the radius of the rolloer.

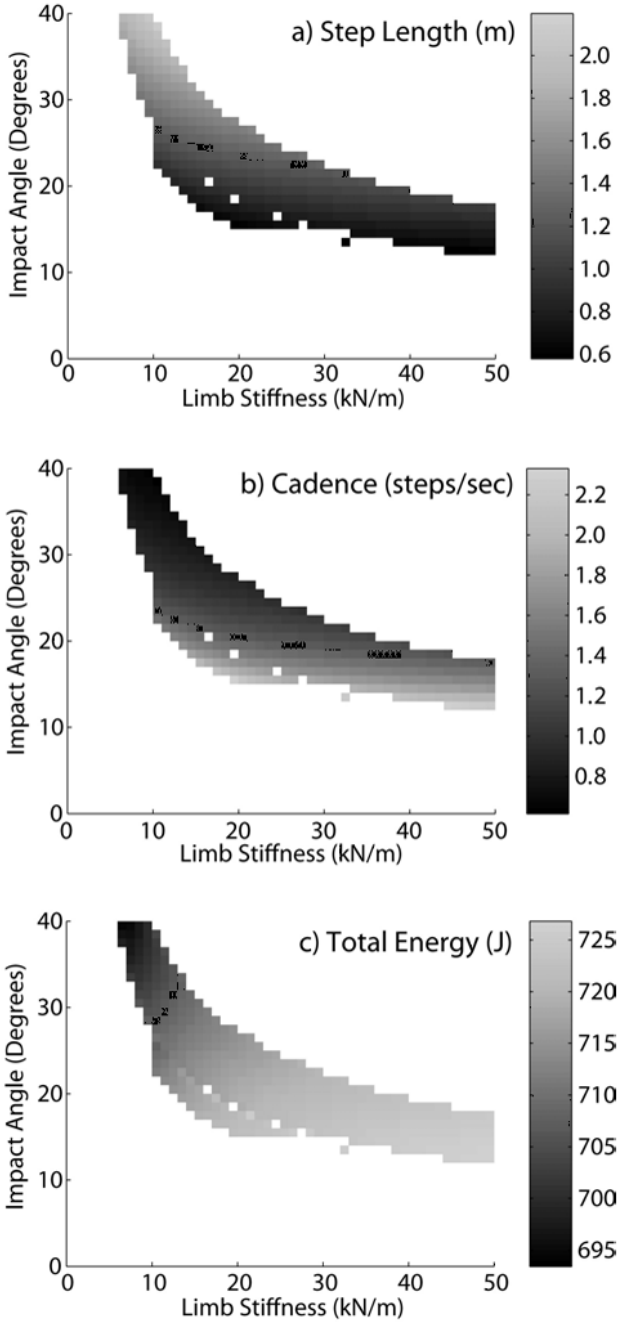

Figure 5.

Shown are the limb stiffness and impact angles that resulted in limit cycle solutions when the 0.3 m roller radius model walked with an average velocity of 1.35 m/s. Each solution exhibits a specific step length (a), cadence (b) and total energy (c). The highest energy states were associated with high cadence-low step length solutions, achieved via coupling high limb stiffness with small impact angles.

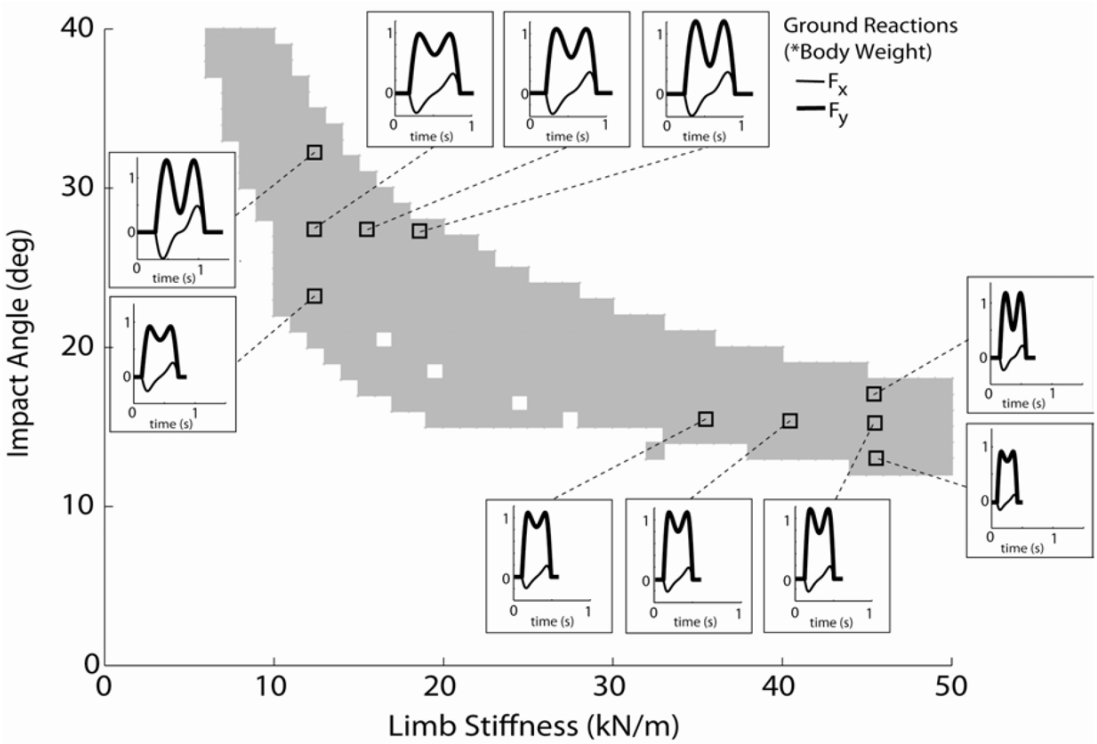

Figure 6.

Variations in limb stiffness and impact angle altered the ground reactions that were induced when walking with a 0.3 m radius roller at an average velocity of 1.35 m/s. An increase in impact angle resulted in larger peak ground reaction forces in both the anterior (F_x) and vertical (F_y) directions, and also substantially prolonged the stance period. Increasing limb stiffness tended to induce slightly larger vertical ground reactions.

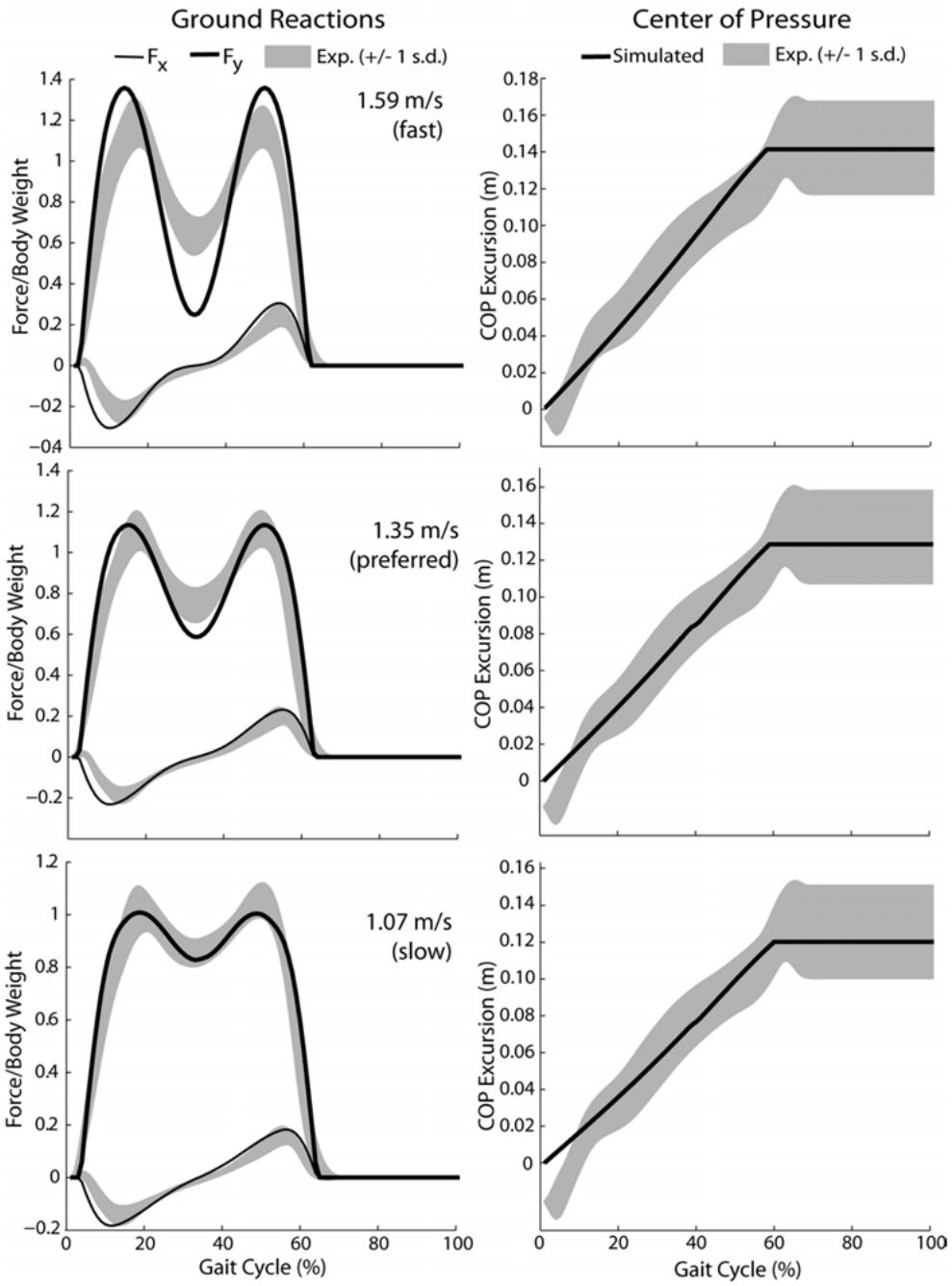

Figure 7.

Use of the model parameters given in Table 1 induced anterior (F_x) and vertical (F_y) ground reaction forces that most closely resembled average experimental (exp) forces at the slow walker speed. At the faster walking speed, the simulated ground reactions exhibited greater variation in stance than seen experimentally. For all speeds, a roller radius of 0.3 m resulted in reasonable approximations of the center of pressure (COP) excursion.

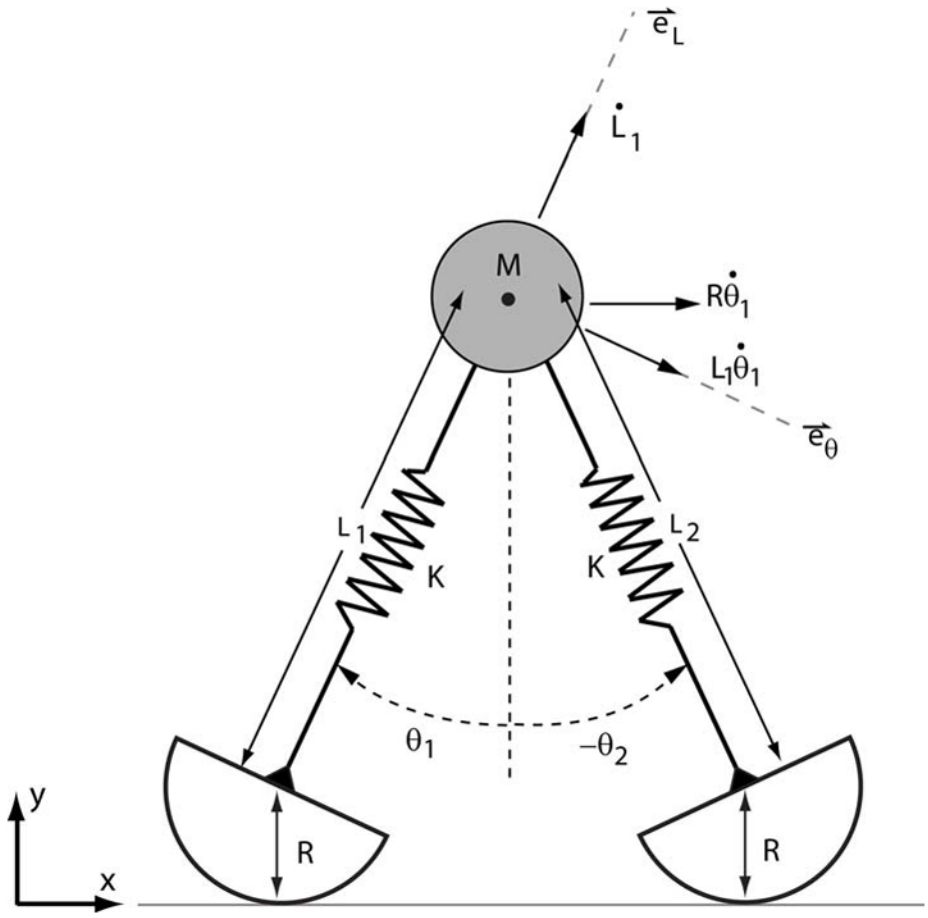

Figure A1.
The velocity of the mass M can be decomposed by components in the forward (x) direction, and both along and perpendicular to the trailing limb.

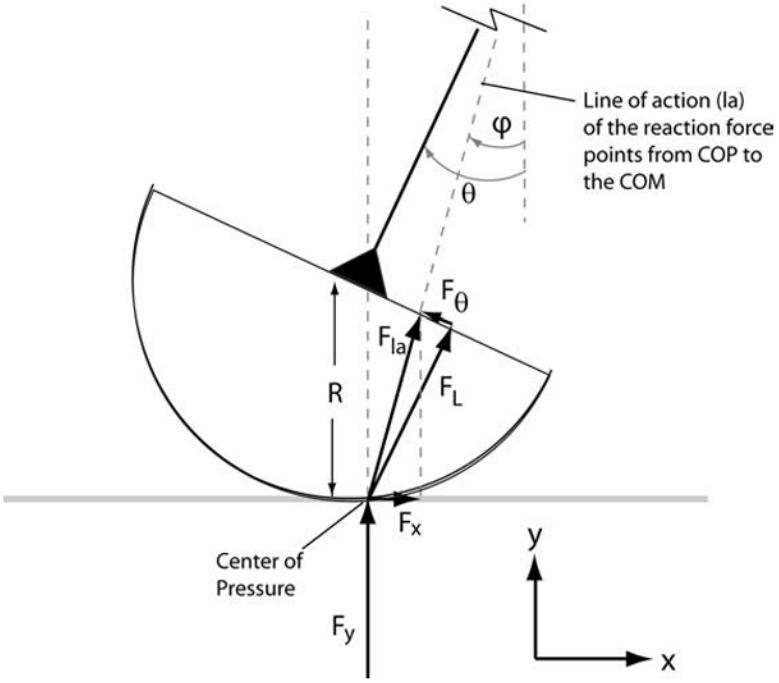

Figure B1.
The ground reaction force vectors F_x and F_y for each limb are computed knowing the spring force F_L and the angle φ that the ground reaction force vector forms with the vertical.

Table 1

Given are the model parameters that produced simulations (sim) that were within one standard deviation of the measured step length and cadence, and best replicated the experimental (exp) ground reactions at each walking speed. Differences between the simulated forces and average measurements were quantified by the root mean squared (rms) error (expressed as % Body Weight) over a gait cycle.

								rms Errors (%BW)	
Speed (% preferred)		**R (m)**	**K (N/m)**	**Θ (°)**	**Speed (m/s)**	**Step Length (m)**	**Cadence (steps/sec)**	**F_x**	**F_y**
80	sim	0.3	21000	23.5	1.07	0.64	1.66	2.8	6.7
	exp				1.06 (±0.11)	0.66 (±0.05)	1.62 (±0.16)		
100	sim	0.3	22000	25.25	1.35	0.70	1.94	4.1	10.8
	exp				1.35 (±0.13)	0.74 (±0.07)	1.83(±0.14)		
120	sim	0.3	24000	27.5	1.59	0.77	2.06	5.5	19.3
	exp				1.59 (±0.14)	0.81 (±0.06)	1.96 (±0.16)		